Outer membrane *c*-type cytochromes OmcA and MtrC play distinct roles in enhancing the attachment of *Shewanella oneidensis* MR-1 cells to goethite during dissimilatory iron reduction

Xinxin Jing[1], Yichao Wu*[,1], Liang Shi[2,3], Caroline L. Peacock[4], Noha Mohamed Ashry[1,5], Chunhui Gao[1], Qiaoyun Huang[1], Peng Cai*[,1]

1 State Key Laboratory of Agricultural Microbiology, College of Resources and Environment, Huazhong Agricultural University, Wuhan, China

2 Department of Biological Sciences and Technology, School of Environmental Studies, China University of Geosciences, Wuhan, China

3 State Key Laboratory of Biogeology and Environmental Geology, China University of Geosciences, Wuhan, China

4 School of Earth and Environment, University of Leeds, Leeds LS2 9JT, UK

5 Agriculture Microbiology Department, Faculty of Agriculture, Benha University, Moshtohor, Qalubia, 13736, Egypt

Supplementary Methods:

Genotypic and phenotypic characterization. PCR amplification and immunolocalization were applied to characterize the genotypic and phenotypic traits of strains used in this study. *mtrC* was amplified with primer mtrC-F (5'-ACTCGCCACGTTGATTCTGT-3') and mtrC-R (5'-ACATGCGTCAAGGCCTACAA-3'). *omcA* was amplified with primer omcA-F (5'-TGGAAAGCCCACGAAAGTGA-3') and omcA-R (5'-CTGCCTAAAGCGATACCCGT-3'). The antibodies against the hydrophilic and surface-exposed regions of MtrC and OmcA were produced as the previous study (1). The amino acid sequences of immunogenic peptides are GCKNGALDPKATIN (MtrC, 399-410) and GCHTEKPSAHHSSTD (OmcA, 349-364).

Iron oxides reduction assays. During the cell-mineral attachment experiment, QCM-D effluent was collected periodically in an acid-washed vial purged with nitrogen gas to prevent Fe(II) oxidized and precipitated. The Fe(II) concentration of QCM-D effluent were measured by the ferrozine assay (Stookey, 1970) after extracted in 0.5 M HCl overnight. Fe(II) concentration were determined using ferrous ammonium sulfate as a standard solution.

Table S1. IR band assignments for *Shewanella*

Wavenumber (cm^{-1})	IR band assignment
1742	υ(C = O) in COOH of OmcA, MtrC(2)
1729−1720	C=O stretch in COOH(3, 4)
1700-1600	amide I: C=O stretching, -CN and –NH bending in amines(5)
1550-1540	amide II: N-H bending, C-N stretching(3-5)
1482-1454	bending of CH_2/CH_3(3, 4)
1450-1360	$\upsilon_s(COO^-)$(3)
1260-1220	$\upsilon_{as}(PO_2^-)$(4)
1160-1150	υ_s(P-O) of phosphoryl surface complexes(5)
1120-1110	υ(P=O)(5)
1118-1114	υ(C-O-P,P-O-P),ring vibrations(3, 4)
1094-1080	$\upsilon_s(PO_2^-)$; ring vibrations; υ(C−O); P=O stretch in phosphodiester, phosphorylated proteins, and polyphosphates(3, 5)
1078-1048	C−OH, C−O−C, and C−C vibrations of polysaccharides(3)
1045	υ(P-OFe)(5)
1043-1039	υ(P-OH,P-OFe)(3, 4)
1020-1016	υ(P-OFe), ring vibrations(3, 4)
1011-995	υ_{as}(P-$(OFe)_2$)(5)
979-962	symmetric stretching of PO_3 and PO_2(3, 5)
955-950	υ(P-OH,P-OFe)(5)
930-927	υ_s(P-$(OFe)_2$)(5)
886	δ(OH) of goethite(5)

Table S2. Signs of each cross-peak in the 2D correlation maps of WT cells during short-term attachment (Figure S7A, B). “0” indicates no cross peak in the position.

	1645	1543	1087	1053	1046
1645	+	+(0)	+(+)	+(+)	+(+)
1543		+	+(+)	+(+)	+(+)
1087			+	+(0)	+(0)
1053				+	+(0)
1046					0

peak intensity: $\upsilon_s(PO_2^-)$(1087 cm^{-1}) > υ(P-OFe)(1053 cm^{-1}) > amide II(1543 cm^{-1})>amide I(1645 cm^{-1})

reaction sequences: $\upsilon_s(PO_2^-)$(1087 cm^{-1}), υ(C−OH/ C−O−C/C−C) (1053 cm^{-1}), υ(P-OFe) (1046 cm^{-1})> amide I(1645 cm^{-1}) , amide II(1543 cm^{-1})

Table S3. Signs of each cross-peak in the 2D correlation maps of WT cells during long-term attachment (Figure S7C, D). “0” indicates no cross peak in the position.

	1645	1546	1398	1076	1048
1645	+	+(+)	+(0)	+(+)	0(+)
1546		+	+(0)	+(+)	0(+)
1458			+	+(+)	0(+)
1398				+	0(0)
1076					0

peak intensity: *υ*(C−OH/ C−O−C/C−C) (1076 cm^{-1}) > amide II(1546 cm^{-1})>amide I(1645 cm^{-1}) >υ_s(COO$^-$)(1398 cm^{-1})

reaction sequences: *υ*(C−OH/ C−O−C/C−C)(1076 cm^{-1}) > amide II(1546 cm^{-1}) > amide I(1645 cm^{-1})

Table S4. Signs of each cross-peak in the 2D correlation maps of Δ*mtrC* cells during short-term attachment (Figure 5A, B). "0" indicates no cross peak in the position.

	1648	1550	1238	1079	1040
1648	+	+(+)	+(+)	+(+)	0(0)
1550		+	+(+)	+(+)	0(0)
1238			+	+(+)	0(+)
1079				+	0(0)
1040					0

peak intensity: $\upsilon_s(PO_2^-)$(1079 cm^{-1})> amide I(1648 cm^{-1}) > amide II(1550 cm^{-1})> $\upsilon_{as}(PO_2^-)$(1238 cm^{-1})

reaction sequences: $\upsilon_s(PO_2^-)$(1079 cm^{-1})> $\upsilon_{as}(PO_2^-)$ (1238 cm^{-1}) > amide II(1550 cm^{-1})> amide I (1648 cm^{-1})

Table S5. Signs of each cross-peak in the 2D correlation maps of Δ*omcA*-Δ*mtrC* cells during short-term attachment (Figure S8A, B). "0" indicates no cross peak in the position.

	1644	1548	1404	1236	1082	1051	1040
1644	+	+(0)	+(+)	+(0)	+(+)	+(+)	0(+)
1549		+	+(+)	+(0)	+(+)	+(+)	0(+)
1404			+	+(-)	+(+)	+(+)	0(+)
1236				+	+(+)	+(+)	0(0)
1082					+	+(0)	0(+)
1051						+	0(+)
1040							0

peak intensity: $\upsilon_s(PO_2^-)$(1082 cm^{-1})>υ(C−OH/ C−O−C/C−C) (1051 cm^{-1})> amide I(1644 cm^{-1}) > amide II(1548 cm^{-1})> $\upsilon_s(COO^-)$(1404 cm^{-1})> $\upsilon_{as}(PO_2^-)$(1236 cm^{-1})

reaction sequences: υ(C−OH/ C−O−C/C−C)(1051 cm^{-1}),$\upsilon_s(PO_2^-)$(1082 cm^{-1}) >$\upsilon_s(COO^-)$(1404 cm^{-1})> amide I(1644 cm^{-1}) >amide II(1548 cm^{-1}), $\upsilon_{as}(PO_2^-)$ (1236 cm^{-1})

Table S6. Signs of each cross-peak in the 2D correlation maps of Δ*omcA* cells during short-term attachment (Figure 6A, B). "0" indicates no cross peak in the position.

	1646	1548	1462	1400	1236	1086	1046	943
1646	+	+(+)	+(+)	+(-)	+(0)	+(+)	+(+)	+(+)
1548		+	+(+)	+(-)	+(-)	+(0)	+(+)	+(+)
1462			+	+(-)	+(-)	+(-)	+(-)	0(0)
1400				+	+(0)	+(+)	+(+)	0(+)
1236					+	+(+)	+(+)	+(+)
1086						+	+(0)	+(+)
1049							0	+(0)
943								+

peak intensity: amide I(1646 cm^{-1}) > amide II(1548 cm^{-1}) > $\upsilon_s(PO_2^-)$ (1086 cm^{-1})> υ(P-OFe) (1046 cm^{-1})> $\upsilon_{as}(PO_2^-)$(1236 cm^{-1}) > $\upsilon_s(COO^-)$(1400 cm^{-1})> $\delta(CH_3/CH_2)$ (1462 cm^{-1}) > υ_s $(P-(OFe)_2)$(943 cm^{-1})

reaction sequences: $\delta(CH_3/CH_2)$ (1462 cm^{-1}) > υ(P-OFe) (1046 cm^{-1}) ,$\upsilon_s(PO_2^-)$(1086 cm^{-1}), amide II(1548 cm^{-1}) > amide I(1646 cm^{-1}) > $\upsilon_s(COO^-)$(1400 cm^{-1})

Table S7. Signs of each cross-peak in the 2D correlation maps of Δ*omcA* cells during long-term attachment (Figure 6C, D). "0" indicates no cross peak in the position.

	1641	1548	1065	1044
1641	+	+(-)	+(-)	0(0)
1548		+	+(-)	0(0)
1065			+	0(0)
				0

peak intensity:*υ*(C−OH/ C−O−C/C−C)(1065 cm^{-1}) > amide II(1548 cm^{-1}) >amide I(1641 cm^{-1})
reaction sequences: amide I(1641 cm^{-1}) > amideII (1548 cm^{-1}) > *υ*(C−OH/C−O−C/C−C)(1065 cm^{-1})

Table S8. Signs of each cross-peak in the 2D correlation maps of Δ*mtrC* cells during long-term attachment (Figure 5C, D). "0" indicates no cross peak in the position.

	1648	1550	1397	1226	1085	1040
1648	+	+(+)	+(-)	+(-)	+(-)	0(-)
1550		+	+(-)	+(-)	+(-)	0(-)
1397			+	+(-)	+(-)	0(0)
1226				+	+(+)	0(-)
1085					+	0

peak intensity: $\upsilon_s(PO_2^-)$(1085 cm^{-1})> amide I(1648 cm^{-1}) > amide II(1550 cm^{-1})> $\upsilon_{as}(PO_2^-)$(1226 cm^{-1}) >$\upsilon_s(COO^-)$(1397cm^{-1})

reaction sequences: amide II(1550 cm^{-1})> amide I(1648 cm^{-1}) > $\upsilon_s(PO_2^-)$(1085 cm^{-1}) > $\upsilon_s(COO^-)$(1397cm^{-1}) > $\upsilon_{as}(PO_2^-)$(1226 cm^{-1})

Table S9. Signs of each cross-peak in the 2D correlation maps of Δ*omcA*-Δ*mtrC* cells during long-term attachment (Figure S8C, D). "0" indicates no cross peak in the position.

	1648	1551	1224	1084	1059	1049
1648	+	+(+)	+(-)	+(-)	+(-)	0(0)
1551		+	+(-)	+(-)	+(-)	0(0)
1224			+	+(+)	+(+)	0(0)
1084				+	+(-)	0(-)
1059					+	0(0)
1049						0

peak intensity: $\upsilon_s(PO_2^-)$(1084 cm^{-1})> υ(C−OH/ C−O−C/C−C) (1059 cm^{-1})> amide I(1648 cm^{-1}) > amide II(1551 cm^{-1}) > $\upsilon_{as}(PO_2^-)$(1224 cm^{-1})

reaction sequences: amide II(1551 cm^{-1}) > amide I(1648 cm^{-1}) > $\upsilon_s(PO_2^-)$(1084 cm^{-1})> υ(C−OH/ C−O−C/C−C) (1059 cm^{-1})> $\upsilon_{as}(PO_2^-)$(1224 cm^{-1})

Table S10. The adhesion forces and rupture length of four strains in AFM analysis. Different letters following the mean values±SE (n=100) indicate significant differences among the strains (P<0.05).

	Adhesion forces (nN)	Rupture length (nm)
WT	1.17±0.05 a	292.33±11.35 a
Δ*mtrC*	1.18±0.05 a	182.64±6.94 b
Δ*omcA*	0.71±0.03 b	99.02±4.80 d
Δ*omcA*-Δ*mtrC*	0.75±0.03 b	132.02±7.43 c

Table S11. Fe(II) concentration of QCM-D effluent during the cell-mineral attachment experiment

	Fe(II) concentration (μg/ml)						
Strain	0 h	0.5 h	1 h	3 h	5 h	8 h	11 h
Abiotic control	0.043±0.005	0.050±0.010	0.035±0.005	0.046±0.013	0.047±0.038	0.054±0.003	0.041±0.005
WT	0.030±0.008	0.045±0.004	0.052±0.008	0.041±0.001	0.041±0.001	0.050±0.005	0.049±0.006
Δ*omcA*	0.036±0.005	0.042±0.002	0.041±0.004	0.047±0.005	0.046±0.005	0.053±0.004	0.051±0.003
Δ*mtrC*	0.068±0.006	0.045±0.001	0.043±0.006	0.051±0.005	0.044±0.002	0.044±0.009	0.048±0.005
Δ*omcA* -Δ*mtrC*	0.032±0.001	0.059±0.002	0.040±0.000	0.040±0.001	0.036±0.001	0.037±0.001	0.039±0.001

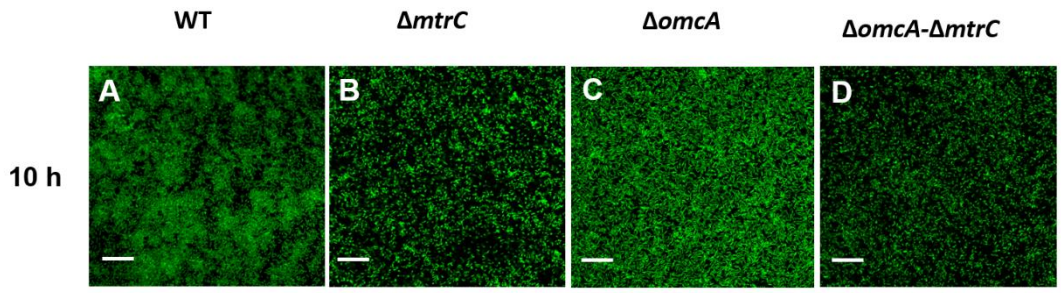

Fig. S1. The microscopic images of QCM-D sensors after 10-h attachment, the bar is 20 μm.

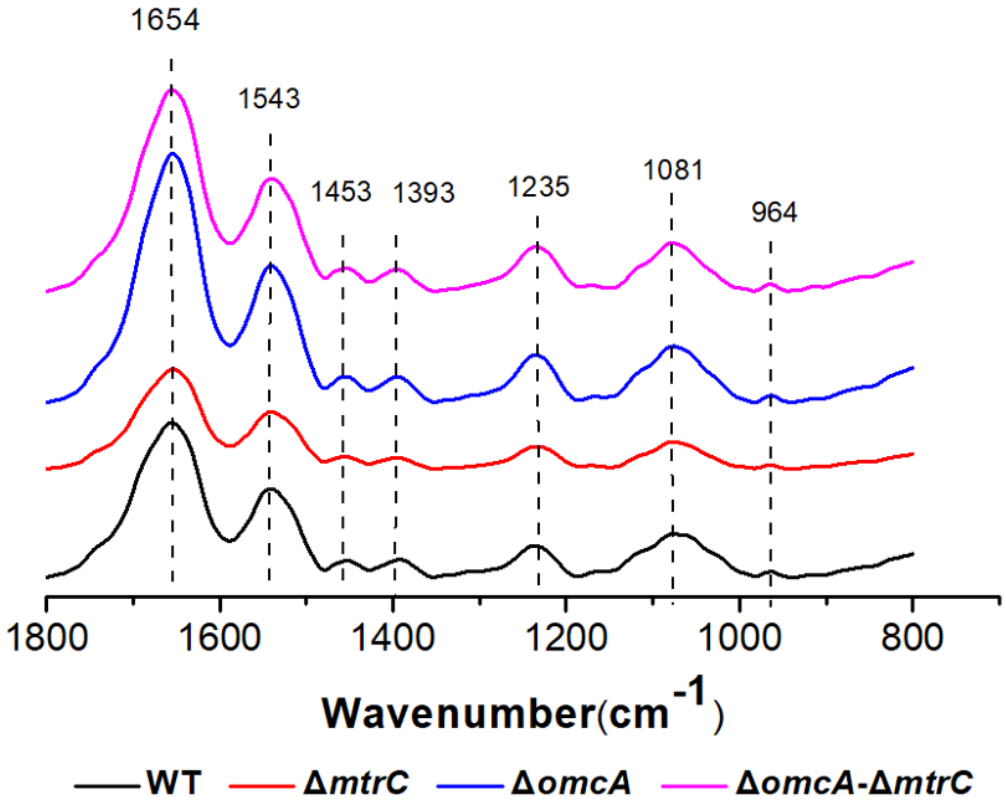

Fig. S2. ATR-FTIR spectra of goethite-free *Shewanella* cells.

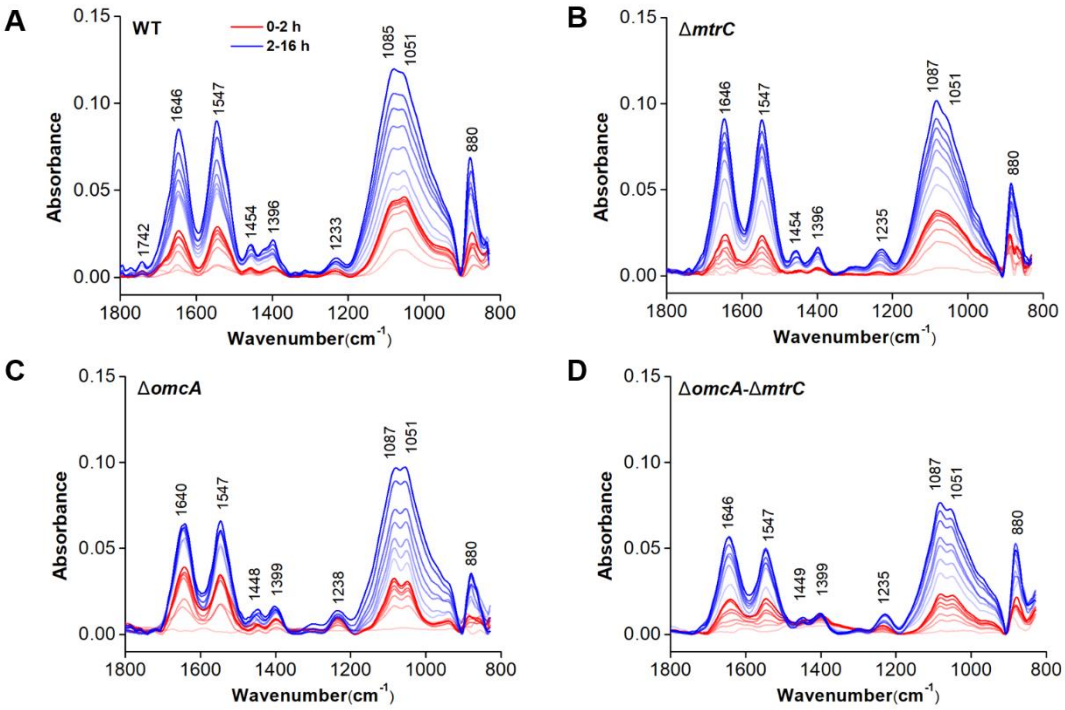

Fig. S3. ATR-FTIR spectra of WT (A), Δ*mtrC* (B), Δ*omcA* (C) and Δ*omcA*-Δ*mtrC* (D) attachment to goethite during short-term (0-2 h) and long-term (2-16 h).

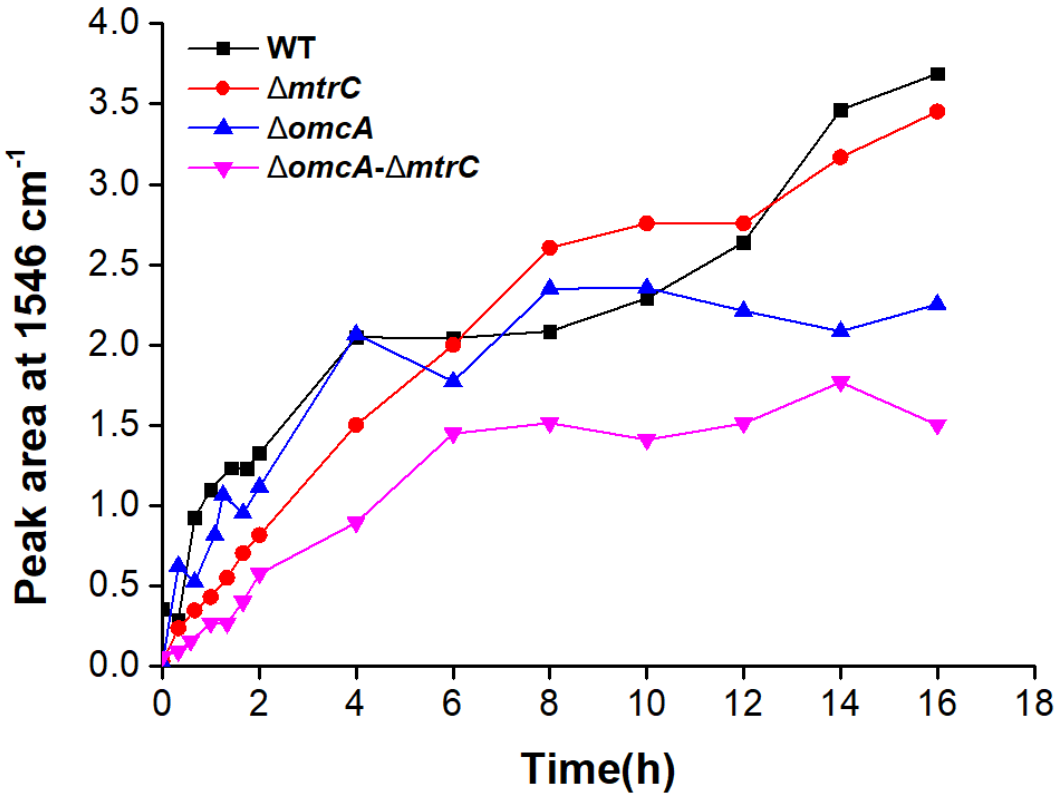

Fig. S4. The changes of peak area for amide II (1543 cm^{-1}) as a function of time.

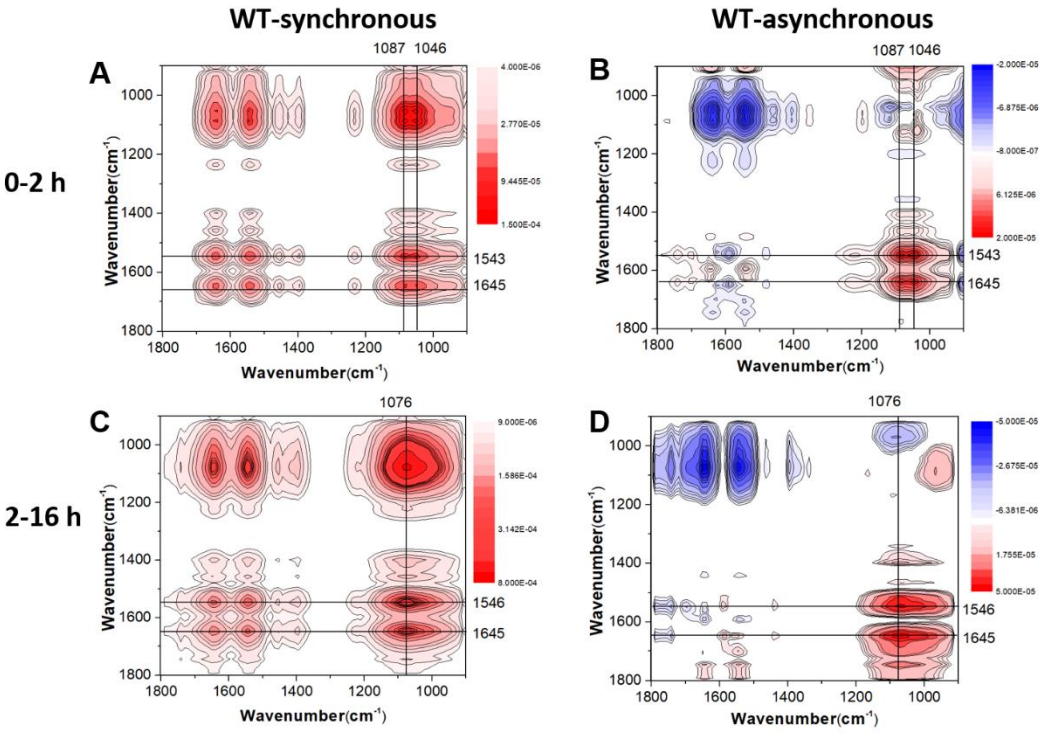

Fig. S5. Synchronous (A, C) and asynchronous (B, D) 2D correlation map of time-dependent ATR-FTIR spectra for the short-term (A, B) and long-term (C, D) attachment of WT cells to goethite. The red and blue regions represent positive and negative correlations intensities.

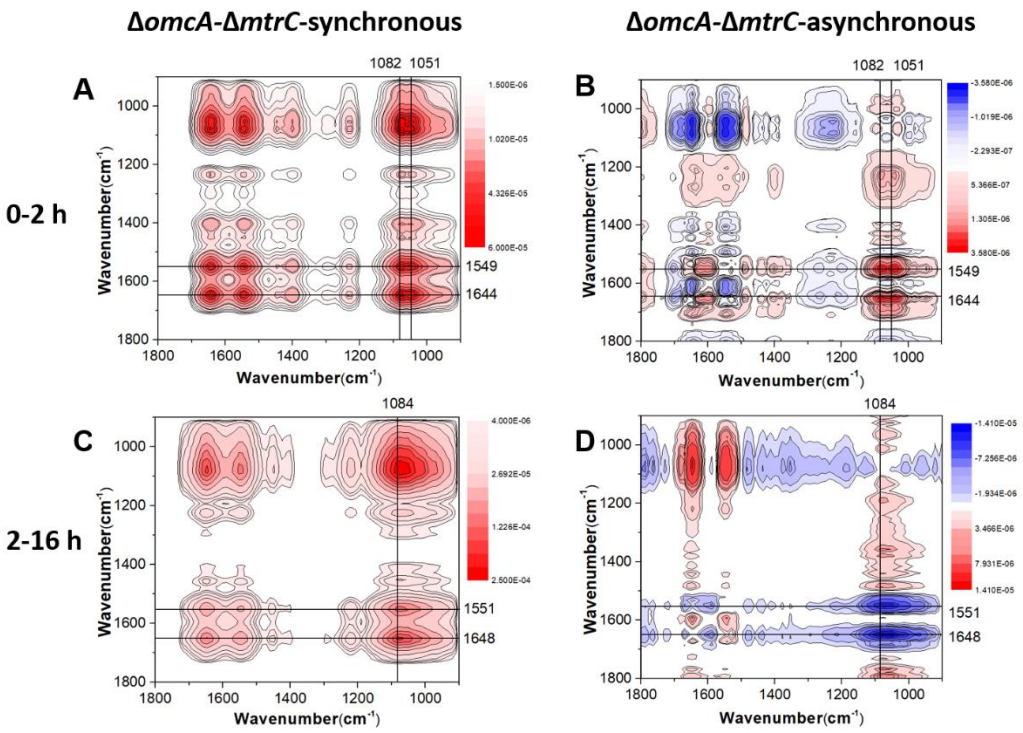

Fig. S6. Synchronous (A, C) and asynchronous (B, D) 2D correlation map of time-dependent ATR-FTIR spectra for the short-term (A, B) and long-term (C, D) attachment of Δ*omcA*-Δ*mtrC* cells to goethite. The red and blue regions represent positive and negative correlations intensities.

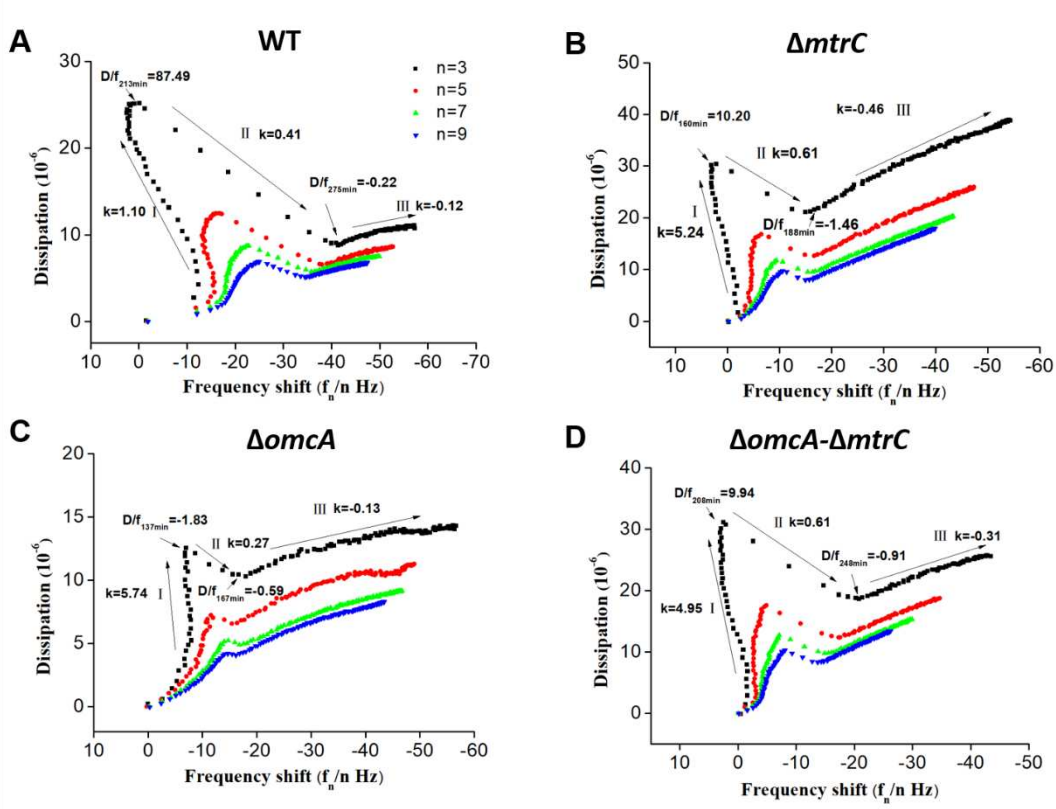

Fig. S7. QCM-D Δ*D*-Δ*f* plots for *Shewanella* cells attached on goethite surface.

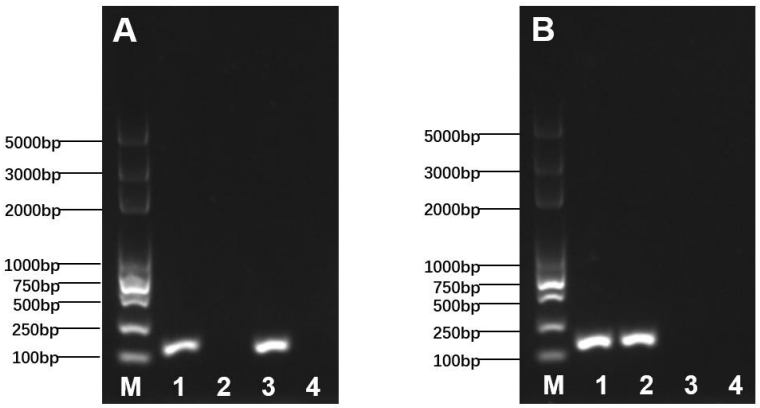

Fig. S8. Validation of PCR products by gel electrophoresis. M: DL5000 marker; Lane 1-4: Amplication frag-ment of the *S. oneidensis* MR-1 WT (1), Δ*omcA* (2), Δ*mtrC* (3), Δ*omcA*-Δ*mtrC* (4) using primer pairs of omcA-F and omcA-R(A), mtrC-F and mtrC-F(B).

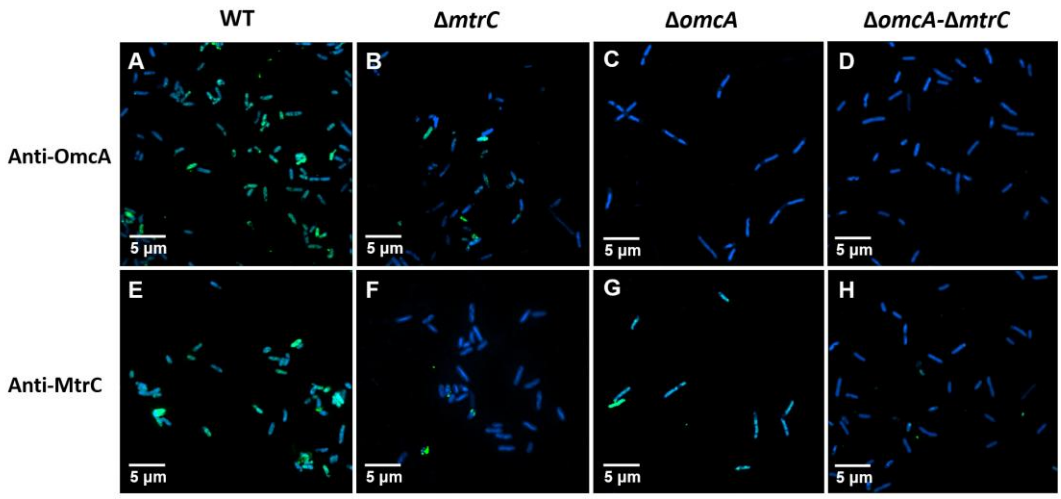

Fig. S9. Structured illumination microscopy images of WT (A, E), Δ*mtrC* (B, F), Δ*omcA* (C, G) and Δ*omcA*-Δ*mtrC* (D, H) stained by DAPI (blue). Outer membrane OmcA and MtrC were specific labeled with antibodies against OmcA (A-D, green) or MtrC (E-H, green).

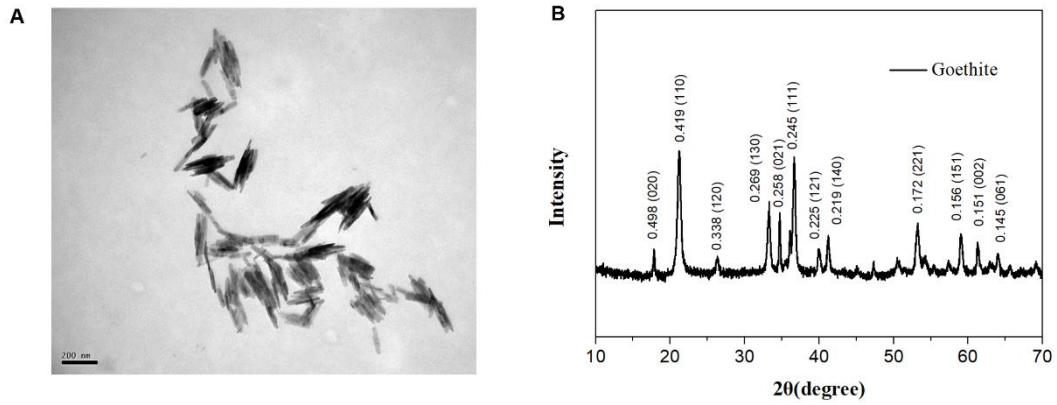

Fig. S10. Transmission electron microscopic (TEM) images of goethite (A). Powder X-ray diffraction (XRD) patterns of goethite (B).

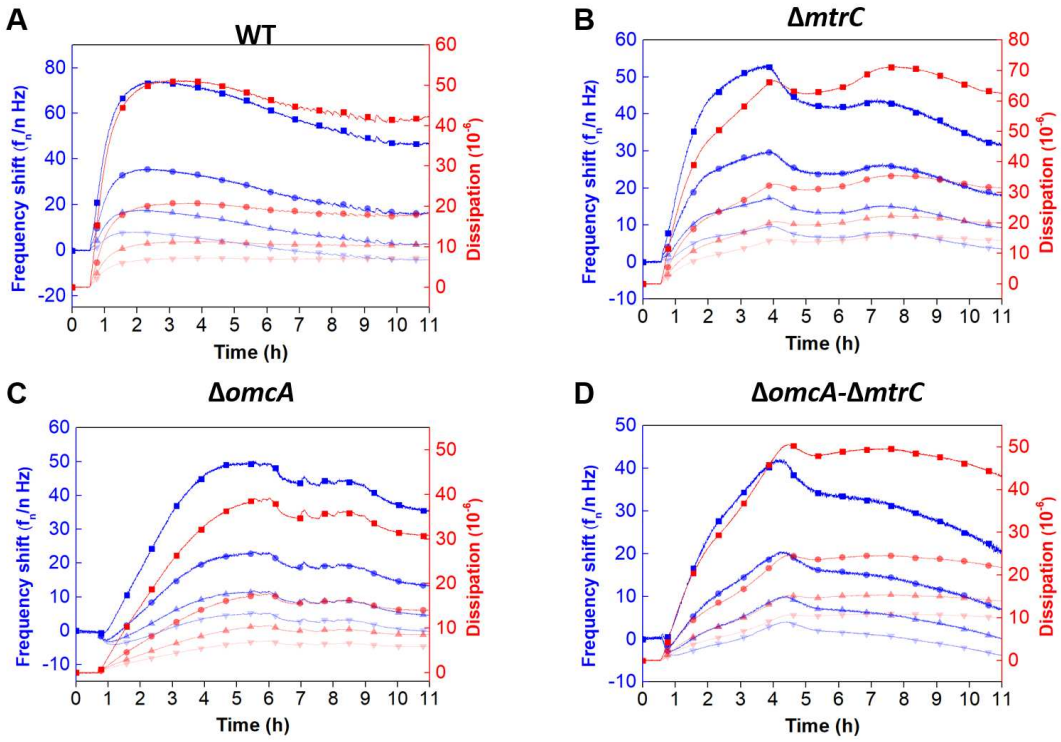

Fig. S11. The frequency (Δf) and dissipation (ΔD) shift for the attachment of WT (A), ΔmtrC (B), ΔomcA (C) and ΔomcA-ΔmtrC (D) on golden sensors.

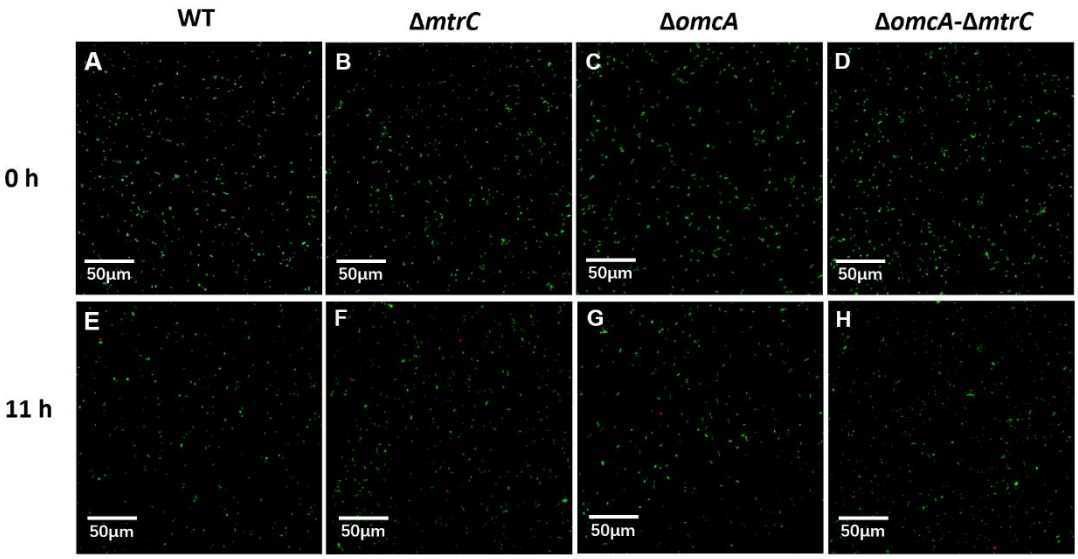

Fig. S12. Fluorescence microscopic images of WT (A, E), ΔmtrC (B, F), ΔomcA (C, G) and ΔomcA-ΔmtrC (D, H) incubated in 0.1 M NaCl for 0 hours and 11 hours.

Reference

1. Marshall MJ, Beliaev AS, Dohnalkova AC, Kennedy DW, Shi L, Wang Z, Boyanov MI, Lai B, Kemner KM, McLean JS, Reed SB, Culley DE, Bailey VL, Simonson CJ, Saffarini DA, Romine MF, Zachara JM, Fredrickson JK. 2006. *c*-Type Cytochrome-Dependent Formation of U(IV) Nanoparticles by *Shewanella oneidensis*. PLOS Biology 4:e268.
2. You LX, Rao L, Tian XC, Wu RR, Wu X, Zhao F, Jiang YX, Sun SG. 2015. Electrochemical in situ FTIR spectroscopy studies directly extracellular electron transfer of *Shewanella oneidensis* MR-1. Electrochim Acta 170:131-139.
3. Elzinga EJ, Huang JH, Chorover J, Kretzschmar R. 2012. ATR-FTIR spectroscopy study of the influence of pH and contact time on the adhesion of *Shewanella putrefaciens* bacterial cells to the surface of hematite. Environ Sci Technol 46:12848-12855.
4. Parikh SJ, Chorover J. 2006. ATR-FTIR Spectroscopy Reveals Bond Formation During Bacterial Adhesion to Iron Oxide. Langmuir 22:8492-8500.
5. Yan W, Wang H, Jing C. 2016. Adhesion of *Shewanella oneidensis* MR-1 to Goethite: A Two-Dimensional Correlation Spectroscopic Study. Environ Sci Technol 50:4343-4349.